POLITECNICO DI TORINO
Repository ISTITUZIONALE

Non-modal stability analysis of the supercritical water reactor lumped model

Original
Non-modal stability analysis of the supercritical water reactor lumped model / Introini, C., Cammi, A., Cervi, E., Savoldi, L.. - In: NUCLEAR ENGINEERING AND DESIGN. - ISSN 0029-5493. - ELETTRONICO. - 446:(2026). [10.1016/j.nucengdes.2025.114627]

Availability:
This version is available at: 11583/3015148 since: 2026-09-03T12:52:00Z

Publisher:
Elsevier

Published
DOI:10.1016/j.nucengdes.2025.114627

Terms of use:

This article is made available under terms and conditions as specified in the corresponding bibliographic description in the repository

Publisher copyright

(Article begins on next page)

26 November 2026

Nuclear Engineering and Design 446 (2026) 114627



Contents lists available at ScienceDirect

Nuclear Engineering and Design

journal homepage: www.elsevier.com/locate/nucengdes





Non-modal stability analysis of the supercritical water reactor lumped model☆

Carolina Introini [a,*], Antonio Cammi [a], Eric Cervi [a], Laura Savoldi [b]

[a] Politecnico di Milano, Department of Energy - Nuclear Engineering Division, Milan, 20156, Italy
[b] Politecnico di Torino, MAHTEP Group - Dipartimento Energia 'Galileo Ferraris', Turin, 10129, Italy

ARTICLE INFO

Keywords:
Non-modal stability theory
Super-critical Water Reactor
Lumped modelling approach
Density Wave Oscillations

ABSTRACT

Compared to commercial reactors and other Generation-IV designs, Super-critical Water Reactors (SCWR) presents the unique feature of super-critical water acting as a coolant. Whereas this choice, in principle, will guarantee higher thermal efficiencies compared to standard light-water designs, thermal-hydraulic instabilities are a cause of concern, since near the thermodynamic pseudo-critical point water properties show significant variability: thus, the study of stability for the SCWR is a primary concern for its future licencing. In this context, this study further expands the analysis of stability of the SCWR using non-modal stability theory: compared to standard modal stability analysis, which focuses on the behaviour of the system, both linear and non-linear, following the exhaustion of the perturbation, non-modal theory studies on the short-term perturbation amplification in linearised systems, thus focusing on the early stages of instability even for asymptotically stable operating states. Being a preliminary work in this sense, this study adopts a simple lumped-parameter model for the SCWR, coupling point-kinetics equations with a mono-dimensional model to describe the core thermal-hydraulics, focusing on the influence of perturbations on various parameters to study their influence on the short-term response of the system. In particular, the presence of power oscillations in the early stages of the transient, potentially related to Density Wave Oscillation instability, is shown.

1. Introduction

The Super-critical Water Reactor (SCWR) is one of the six concept selected by the Generation-IV International Forum (Gen-IV International Forum, 2023). It uses super-critical water as a coolant, since it theoretically allows for reaching higher thermal efficiencies (due to the increased temperature and pressure) of around 45% (Ortega Gomez, 2009) without exhibiting Departure from Nucleate Boiling (DNB), which limits the operating temperature of traditional Light Water Reactors (LWR). Operating at a pressure of around 25 MPa, the coolant water can reach an average outlet temperature of 500 °C, and the hot steam can be sent to the turbine with a direct cycle. Contrary to Boiling Water Reactors (BWR), no boiling occurs, and the outlet coolant remains single-phase, meaning that no steam separators or recirculation pumps are needed. However, two major challenges arise. Due to the higher pressure and temperature, the core will deal with more severe mechanical conditions (such as higher mechanical stresses and higher thermal loads), whereas the materials exhibit lower mechanical strength due to the higher temperature. The other concern is represented by thermal-hydraulic instabilities: near the thermo-dynamic super-critical point, water experiences a significant decrease in density, and due to the large temperature difference between inlet and outlet this drop is larger than in BWR: therefore, even if boiling does not occur, the SCWR may be subjected to all the instability phenomena that occur in two-phase systems (Schulenberg and Laurence, 2023). Fig. 1 shows some (normalised) properties of water in the region near the super-critical point, at 22.06 MPa and 373.9 °C. The region where the thermo-dynamic properties exhibit rapid changes is called pseudo-boiling region, which has an extension of about 50 °C for water (Zhao, 2005).

Due to the significant density drop in the pseudo-boiling region, Density Wave Oscillations (DWO) are the most concerning of all the two-phase flow instabilities for SCWR. DWO is a dynamic instability (Ortega Gomez, 2009) that is characterised by an oscillating response of the system to slight variations in the inlet flow. Fig. 2 illustrates the mechanics of this time-delay feedback instability, caused by the finite velocity of the channel fluid flow. Since the fluid travels through the heated channel at a finite speed, the first peak of the

☆ This article is part of a Special issue entitled: 'ISSCWR-11' published in Nuclear Engineering and Design.

* Corresponding author.
E-mail address: carolina.introini@polimi.it (C. Introini).

https://doi.org/10.1016/j.nucengdes.2025.114627
Received 27 August 2025; Received in revised form 16 October 2025; Accepted 18 November 2025
Available online 20 November 2025
0029-5493/© 2025 The Authors. Published by Elsevier B.V. This is an open access article under the CC BY-NC-ND license (http://creativecommons.org/licenses/by-nc-nd/4.0/).

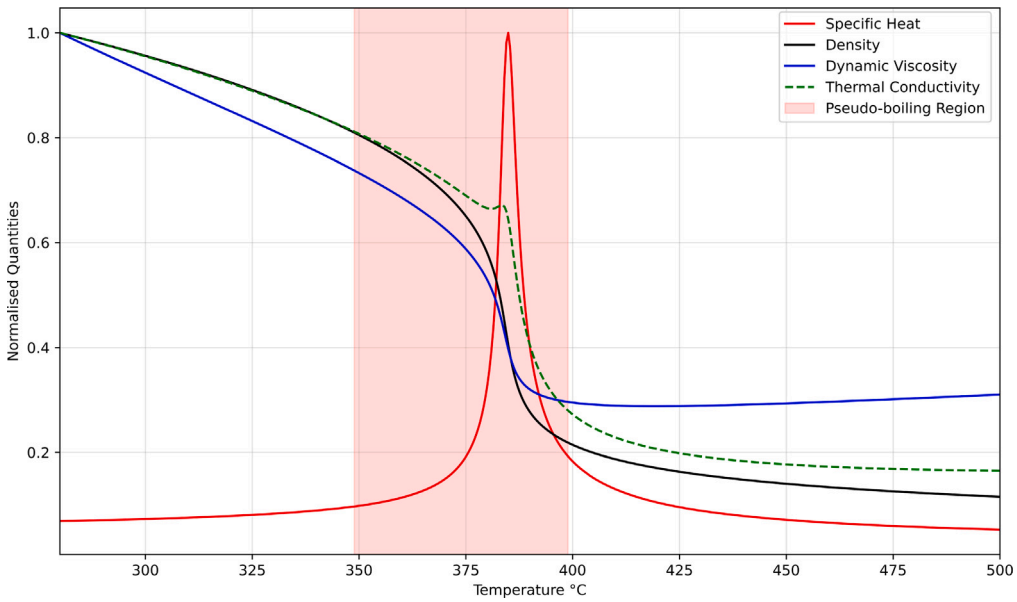

Fig. 1. Normalised specific heat (red), density (black), dynamic viscosity (blue) and thermal conductivity (green) for water at 22.06 MPa, near the super-critical point (T_{sc} = 373.9 °C: in the pseudo-boiling region ($T_{sc}\pm$ 30), sharp variations in the thermo-physical properties can be observed. In particular, between inlet (280 °C) and outlet (500 °C) temperature, density decreases by more than 80%.

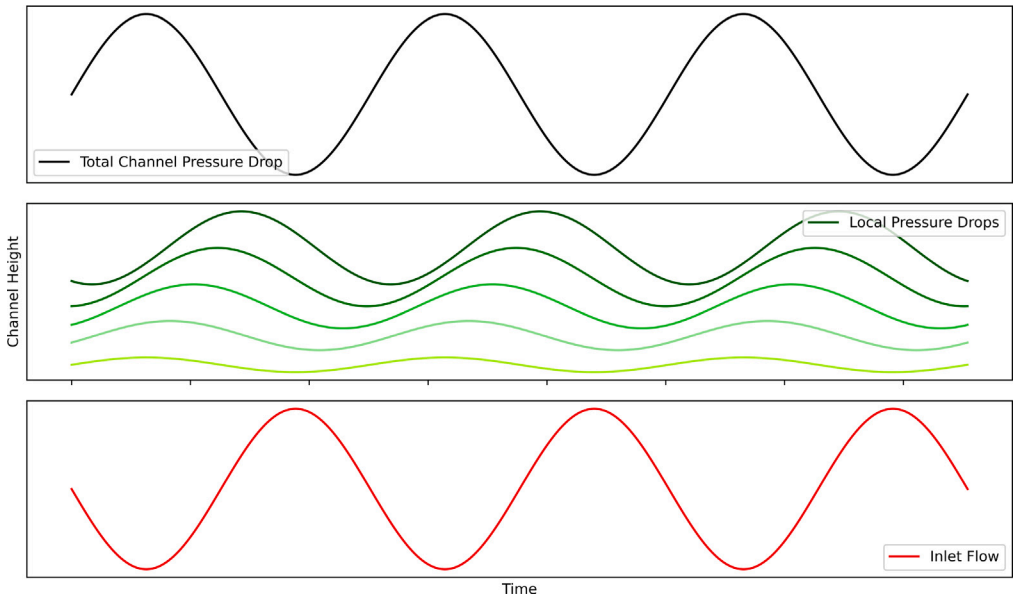

Fig. 2. Mechanism of DWO instabilities: a (for example) sinusoidal inlet flow perturbation causes a sinusoidal local pressure drop, whose amplitude increases with increasing axial length: due to the finite velocity of the fluid, the first peak of the oscillation has a time delay compared to higher axial positions. The total pressure is sinusoidal as well, and if the delay becomes 180° of the inlet flow fluctuation, the two becomes in counter-phase, giving a positive feedback effect.

oscillation will be delayed in time compared to peaks in higher positions. For instance, if the inlet flow perturbation is sinusoidal, the local pressure drops will also be sinusoidal, with amplitude increasing with the axial length (Yadigaroglu, 1970). In particular, the feedback will become positive if the delay reaches 180° at a particular frequency (which depends on the dimensions of the channel), meaning that the inlet flow fluctuations and pressure drop oscillations are in counter-phase. This will lead to self-sustaining oscillations and an unstable operating point.

In a nuclear reactor, the neutron flux, and thus the generated power, is affected by the coolant density through the reactivity feedback coefficients. Therefore, a density fluctuation in the coolant causes a fluctuation in the power in accordance with the neutronic feedback (March-Leuba, 1992). This process leads to the emergence of coupled neutronic thermal-hydraulic (or reactivity) instabilities, which involve two feedback loops: one is common to the DWO and the coupled instability, while the other is a nuclear phenomenon that manifests solely in the reactivity instability. A power excursion results in a variation of the water density; within the thermal-hydraulic block, momentum dynamics control the inlet flow feedback through pressure drop constraints. Subsequently, these thermal-dynamic effects return to the neutronic block via the fuel and moderator feedback reactivity coefficients, thereby influencing the neutron flux. If the density feedback is sufficiently strong, the reactivity and consequently the power may begin to oscillate. These oscillations can be either global or local: in the latter scenario, oscillations are confined to a single channel while the bulk flow remains stable. In such instances, the neutronic feedback

can be disregarded, allowing for the decoupling of neutronics from thermal-hydraulics.

It is clear then how the stability analysis of the SCWR is a key step for understanding this reactor design. Usually, stability analysis of nuclear reactors is performed using linear, modal methods, such as the root locus criterion (Cervi and Cammi, 2018) and Lyapunov stability theory (Nise, 2010), which focus on the asymptotic behaviour following a perturbation. However, this kind of analysis completely neglects the short-term behaviour of the system immediately following the perturbation, especially for non-linear systems with non-orthonormal operators. Indeed, due to the sharp variations in the thermo-dynamic properties in the pseudo-boiling region, supercritical water properties cannot be considered constant within the coolant channel and the moderator water rod, adding another layer of non-linearity to the model describing the SCWR core, thus needing non-linear and non-modal stability approaches.

Among the various approaches for stability analysis, this work adopts the non-modal stability theory developed in Schmidt (2007) for the study of the transition Reynolds umber for enclosed shear flows. Compared to modal methods, which focus only on the long-term stability of the system, the non-modal theory considers also the short-term behaviour over a limited-time interval. Indeed, stability over finite-time intervals is remarkably different from the traditional concept of Lyapunov stability, offering a different viewpoint. Despite this, the use of non-modal stability analysis for studying the dynamics of nuclear reactors is still not widespread, especially for Generation-IV reactor concepts. Previously, the authors applied non-modal stability analysis to a lumped model of the Pressurised Water Reactor, confirming the occurrence of transient phenomena immediately after the perturbation that linear stability analysis cannot see Introini et al. (2020). In general, literature regarding the application of non-modal stability analysis is quite scarce. Other than the aforementioned work, the author also participated in Lo Verso et al. (2024), which applied non-modal stability theory to magneto-hydrodynamic flow in a pipe.

To the best of the author knowledge, most stability analysis of the SCWR focuses on asymptotic stability studies, both linear and non-linear, starting from the initial works of Ambrosini regarding fluid-dynamic stability in supercritical systems (see, for example, Ambrosini and Sharabi (2008)). Other analyses include (Cai et al., 2009) for the start-up phase of the plant, Dutta and Doshi (2009) for the analysis of nuclear-coupled DWO instabilities for the BWR, Paul (2019) for the coupled nonlinear instabilities in the SCWR design, Singh et al. (2021) for its study of nonlinear instabilities in a supercritical heated channel (and Su et al. (2013) for its theoretical study). More recent works include the nonlinear analysis of supercritical parallel channels in Singh et al. (2022).

The structure of the paper is reported below. Following the above brief discussion on instabilities in the SCWR, Section 2 briefly introduces non-modal stability theory, without entering into the mathematical details but focusing on the key differences compared to modal stability. Section 3 then describes, in a qualitative manner, the adopted 1D model: the non-linear equations and subsequent linearisation are reported in the companion Appendix. Section 4 then presents the key results obtained in the analysis, followed by Section 5 where the main findings, some engineering considerations and future works are briefly exposed.

2. Non-modal stability theory

In modal stability analysis, the study of the eigenvalue problem associated with a linearised initial-value problem allows describing the asymptotic behaviour of the system, and just a single unstable mode is considered enough to classify the initial state as unstable. However, especially for strongly non-linear systems, this asymptotic behaviour may not be enough to describe the actual perturbation dynamics, because this asymptotic state may be reached by the system well after the useful intervention time. Indeed, how the system eventually reaches the asymptotic stable state is also relevant, meaning that the study of the single least stable mode, as done by modal stability analysis, is not enough. In fact, modal stability theory says nothing about the short-time behaviour of the linearised initial value problem, which may differ from the asymptotic one (Schmidt and Henningson, 2001).

Fig. 3 reports the three possible stability scenarios: an asymptotically stable transient (red), and asymptotically unstable transient (green), and an asymptotically stable transient exhibiting initial growth of the perturbation (blue). As a matter of fact, non-negligible short-term energy amplification may occur even for systems with no predicted long-time disturbance growth, and this energy growth may amplify small disturbances onto ones that may trigger the transition from a stable to an unstable state. Instead of considering the single mode, non-modal stability analysis considers the behaviour of a mixture of normal modes, of which the possible mutual non-orthogonality may lead to short-term energy growth. Instability is here studied over a finite-time interval to identify the most growing perturbations and to describe how they evolve in time. Stability is here defined more broadly as the response of the system to certain input variables, which may be initial conditions, external disturbances, internal uncertainties, to identify those which result in the largest amplification of the disturbance magnitude.

Detailed discussions on non-modal stability can be found in Schmidt (2007), Trefethen (1997). For completeness, in the following the key theoretical concepts are summarised. Considering only the response to perturbations on the initial conditions, the general solution for the initial-value problem is given by the Lagrange formula:

$$y(t) = \mathbf{C}e^{\mathbf{A}t}\mathbf{B}y_0, \tag{1}$$

where, as in state-space theory (Nise, 2010), $\mathbf{C}$ is the output matrix, relating the state variables $\mathbf{x}$ with the output quantities $\mathbf{y}$, $\mathbf{A}$ is the system matrix and $\mathbf{B}$ is the input matrix. Following hydrodynamic stability theory (Ruban et al., 2023), the maximum amplification $G(t)$ of the perturbation energy in a defined time interval can be computed:

$$G(t) = \max_{y_0} \frac{\|y(t)\|_2^2}{\|y_0\|_2^2} = \max_{y_0} \frac{\|\mathbf{C}e^{\mathbf{A}t}\mathbf{B}y_0\|_2^2}{\|y_0\|_2^2} = \|\mathbf{C}e^{\mathbf{A}t}\mathbf{B}\|_2^2. \tag{2}$$

Eq. (2)[1] describes the maximum energy amplification over all possible initial conditions: to retrieve the specific initial perturbation that causes the maximum possible amplification $G(t_k)$, techniques such as Singular Value Decomposition (SVD) can be used (Trefethen and Embree, 2005). Linear stability theory characterised the growth of disturbances considering only the least stable mode of $\mathbf{A}$: this corresponds to substituting Eq. (2) with the following:

$$g(t) = \|\mathbf{C}e^{2\omega_1 t}\mathbf{B}\|_2^2, \tag{3}$$

where ω_1 is the real part of the least stable eigenvalue of $\mathbf{A}$. Considering the eigenvalue decomposition $\mathbf{A} = \mathbf{W}\boldsymbol{\Lambda}\mathbf{W}^{-1}$, by taking only the eigenvalues of $\mathbf{A}$ for stability analysis the information contained in $\mathbf{W}$, that is, the eigenfunctions of $\mathbf{A}$ is neglected. Instead, by considering the maximum energy amplification $G(t)$, this information is retained, since:

$$G(t) = \|\mathbf{C}e^{\mathbf{A}t}\mathbf{B}\|_2^2 = \|\mathbf{C}\mathbf{W}e^{\boldsymbol{\Lambda}t}\mathbf{W}^{-1}\mathbf{B}\|_2^2, \tag{4}$$

where $\boldsymbol{\Lambda}$ is the diagonal matrix of the eigenvalues.

Now, spectral analysis deals with the real part of the least stable eigenvalue, describing the time-evolution of the norm of the matrix exponential for unitary matrices $\mathbf{W}$: in this case, $g(t) \equiv G(t)$. However, many operators are non-normal and thus their eigenfunctions are non-orthogonal (Reddy et al., 1993): in this case, $g(t) \neq G(t)$, and studying ω_1 is not enough to fully capture the general disturbance behaviour in time nor to describe the behaviour in the early stages of the transient. Indeed, systems characterised by non-normal matrices

[1] All norms in Eq. (2) refer to Euclidean norms.

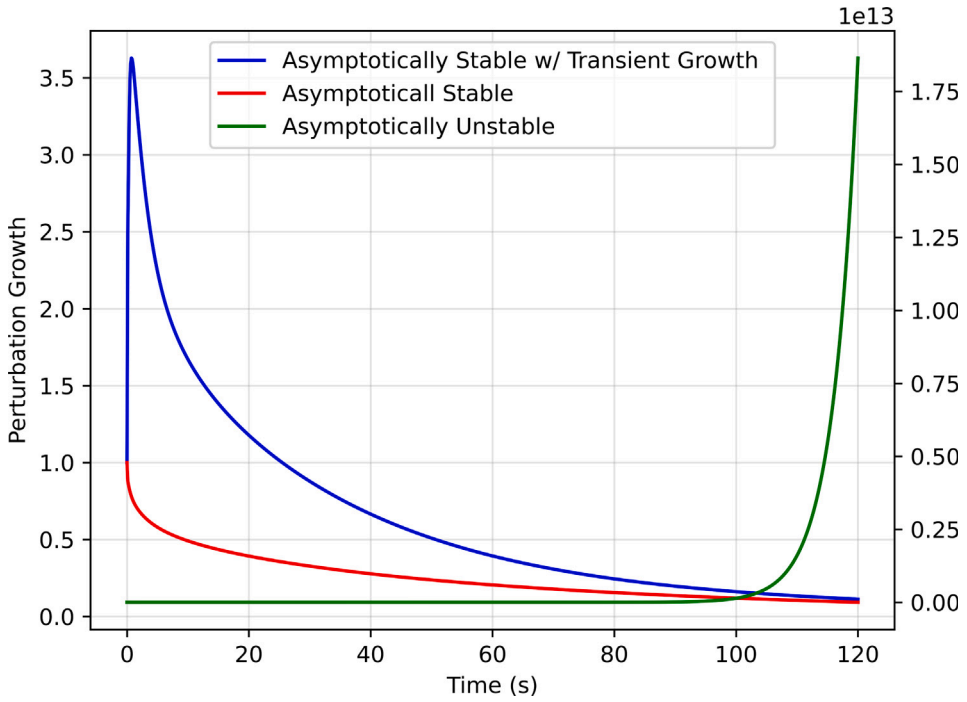

Fig. 3. Examples of transient scenarios: monotonic asymptotically stable (red), unstable (green) and asymptotically stable with initial transient growth (blue): even for eventually stable scenarios, initial growth of the perturbation may occur, which could bring some quantities of interest above their safety threshold for some finite periods of time.

may be subjected to short but large amplification of energy following a perturbation of the initial condition. Therefore, if the eigenvectors of the dynamic matrix **A** form a non-orthogonal set, a transient increase of energy may occur even when the least stable eigenvalue has negative real part. To capture the transient behaviour of the infinitesimal disturbances, the norm of the matrix exponential $G(t)$ must be considered, and therefore a different quantity other than the eigenvalues must be introduced. Considering a Taylor expansion of the matrix exponential around $t = 0^+$ (Marquez, 2003):

$$\max_y \frac{1}{\|y\|^2}\frac{d\|y\|^2_{t=0^+}}{dt} = \max_y \frac{1}{\|y\|^2}\frac{d}{dt}\left\|\mathbf{C}\left(\mathbf{I}+\mathbf{A}t+\frac{\mathbf{A}^2t}{2!}+\cdots\right)\mathbf{B}y_0\right\|^2_{t=0^+} \quad (5)$$
$$= \omega_1(\mathbf{Q}^\mathbf{H}+\mathbf{Q}),$$

where $\mathbf{Q} = 1/2 \cdot \mathbf{CAB}$. The quantity $\omega_1(\mathbf{Q}^\mathbf{H} + \mathbf{Q})$ is called numerical abscissa, and it represents the maximum extension of the numerical range[2] into the right half-plane, and which determines the energy increase. Further insights on the largest short-time energy growth are given by the ε-pseudospectra (Trefethen, 1997), regions in the complex plane, parametrised by ε where the resolvent norm $\|\mathbf{C}(z\mathbf{I}-\mathbf{A})^{-1}\mathbf{B}\|$ is larger than $1/\varepsilon$. A pseudospectrum of an operator is a set containing the spectrum of the operator plus its pseudo-eigenvalues. Mathematically, the ε-pseudospectrum of the matrix **A** consists of all eigenvalues of all matrices which are ε-close to **A**:

$$\Lambda_\varepsilon(\mathbf{A}) = \{\omega \in \mathbb{C} | \exists \mathbf{E} \in \mathbb{C}^{n\times n} : (\mathbf{A}+\mathbf{E})x = \omega x, \|\mathbf{E}\| \leq \varepsilon) \quad (6)$$

Alternatively, the ε-eigenvalues are the eigenvalues of the operator **A** + **E**, where **E** is the disturbance of the norm ε: as ε goes to zero, the regular spectrum can be retrieved (Trefethen, 1997).

3. The SCWR model

The reference design used in this work (Buongiorno and MacDonald, 2003) is based on a direct cycle operating at a pressure of 25 MPa, with thermal power 3575 MW_{th} and net electric power of 1.6 GW_e. The water flows into the core at 280 °C and exits at 500 °C, with a density drop between inlet and outlet nozzles going from 780 kg/m^3 to 90 kg/m^3. Due to the low density of the moderator in the upper part of the core, water rods are needed to ensure enough moderation. For this reason, the inlet flow splits into two parts: 10% of the total flow (roughly 1843 kg/s) goes down through the downcomer, placed between the core and the reactor pressure vessel; the other 90% of the water flows downward through the water rods. The two flows mix in the lower plenum, and the water is then guided upward through the coolant channels.

The model of the SCWR was developed and discussed in detail in Cervi and Cammi (2018). Briefly, the SCWR core investigated here includes 145 fuel assemblies, 5220 water rods and an even larger number of paths for the coolant, which flows in the space between the fuel pins. All these flow paths are collapsed into a single lumped channel, formed by an aggregated control rod and an aggregated coolant channel, which transfer heat through a steel surface. The coolant removes the heat produced by fission and, in turn, transfers heat to the water rod; hence, the SCWR core can be imagined as a counter-flow heat exchanger. A mono-dimensional description as a first approximation for the SCWR is needed because the thermo-physical properties of supercritical water change significantly from point to point and, even for a fixed point, are strongly influenced by the operating conditions of the channel. Hence, the fuel, the coolant channel, the steel surface[3] and the water rod are divided in $M = 487$ nodes, each with a length of $dz = 1$ cm.[4] A schematic of the model is reported in Fig. 4. Regarding the convective heat transfer between the supercritical flow and the wall, following the analysis in Cervi (2016), the Mokry correlation (Pioro and Mokry, 2011) was used: more details can be found in Appendix.

[2] The numerical range of an $n \times n$ matrix **A** is the collection of complex numbers of the form $\mathbf{W} \cdot \mathbf{AW}$, where $\omega \in \mathbb{C}^n$ is a unit vector.

[3] Thus including wall energy storage

[4] This node height was selected to have constant thermo-dynamic properties within the node itself, thus resulting in a total of 487 nodes of height 1 cm each. A sensitivity analysis on the nodalization can be found in Cervi and Cammi (2018).

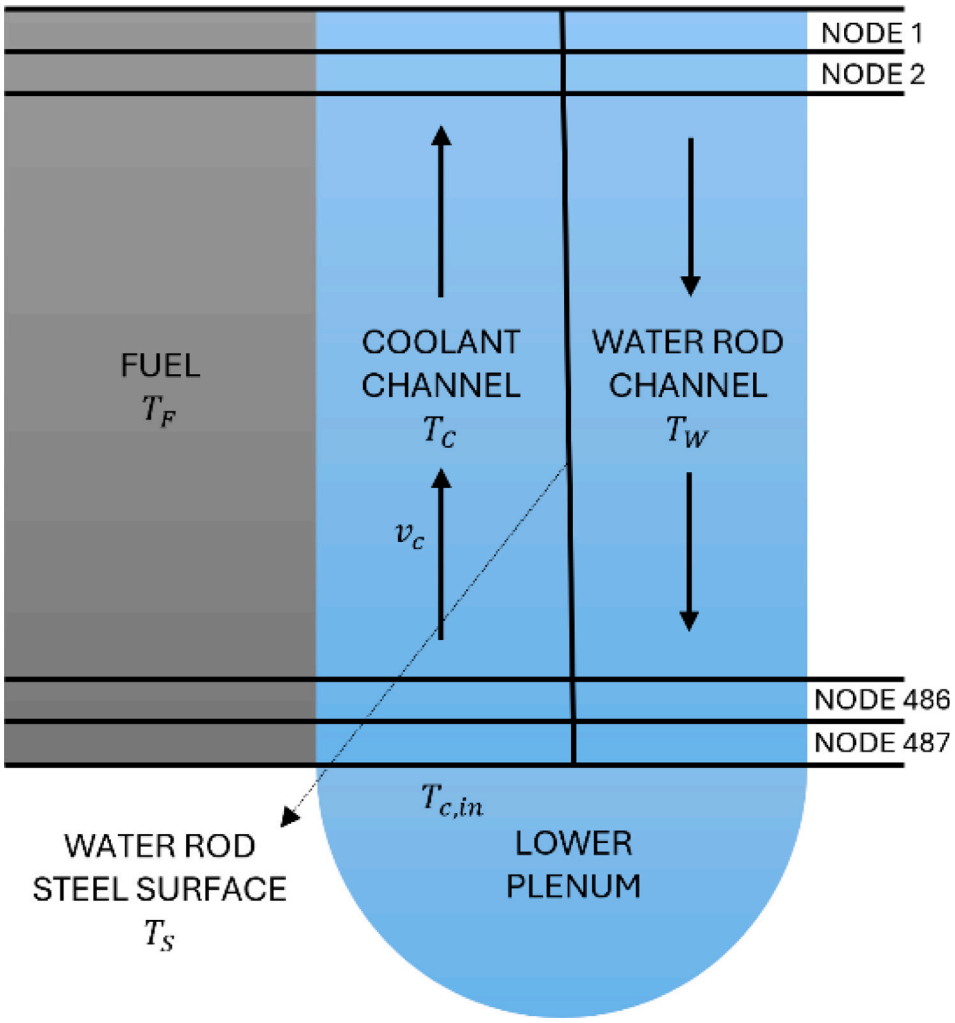

Fig. 4. Schematic of the mono-dimensional, lumped channel model for the SCWR core. Water flows downward from node 1 to node M in the water rod channel and upward from node M to node 1 in the coolant channel, hence the system operates in counter-flow.

The model is non-linear, since the thermo-dynamic properties of water depends on the temperature itself, which is the unknown of the problem. This non-linearity is solved by computing the thermo-dynamic properties of the ith node at the coolant outlet and water rod inlet temperatures, instead of at the representative coolant and water rod node temperatures: this approximation is acceptable due to the fine axial discretisation adopted. The value for the core outlet temperature T_{out} is found through an iterative procedure (Cervi and Cammi, 2018), allowing for solving the nodal energy balances in sequence from the upper node downward. The model has the following boundary conditions (see Cervi (2016) for a more accurate discussion): (1) water rod inlet temperature $T_{w,in} = 280$ °C, representing the out-of-core energy dynamics; (2) external reactivity ρ_{ext} inserted by movement of the control rods (in free dynamics, set equal to zero); (3) constant downcomer conditions $\dot{m}_d h_d$ (the latter equal to the last node of the coolant channel); (4) constant pressure drop ΔP_p between the feedwater pump and the turbine control valve, which depends on the velocity and density of the coolant and the water rod channel, as well as on the exit valve coefficient. More details on the evaluation of the pressure drop can be found in Appendix.

Additional complexity is given by the counter-flow heat transfer that takes place between the coolant channel and the water rods and by the presence of the lower plenum, where the water rods and the downcomer flows are mixed with different values of the specific enthalpy. The other main characteristics of the model are reported below:

- Instantaneous mixing approximation for the lower plenum, thus neglecting the time delay of the mixing.
- Constant pressure drop ΔP_p between the feedwater pump and the turbine control valve for the out-core dynamics, which also includes the pump gain and the exit valve pressure drop.
- An axial cosine profile is adopted for the shape of the total power.

Following linearisation of the model equations and neglecting the superior order infinitesimals, the free-dynamics matrix $\mathbf{A}$ can be retrieved, upon which non-modal stability analysis can be performed. All the equations describing the model, along with their linearisation, are reported in Appendix.

4. Numerical results

The analysis of the non-modal stability study begins considering some generic perturbation of the dynamic matrix $\mathbf{A}$ around the steady state, under the assumption that, following the linearisation of the set of equations, all parameters are independent from the state variables. As mentioned in Section 2, the asymptotic stability of the system is given by the eigenvalues of $\mathbf{A}$, the eleven largest of which are reported in Fig. 5: in modulus, the maximum eigenvalue is $Re(\omega_1) = -0.0036$, belonging to the first complex conjugate eigenvalues pair $\omega_1 = \omega_1^\star = -0.0036 \pm 0.036i$, confirming asymptotic stability (highlighted in red); the presence of pairs of complex conjugate eigenvalues, instead, confirm the oscillatory behaviour of the SCWR related to the behaviour of the thermo-dynamic properties near the critical point.

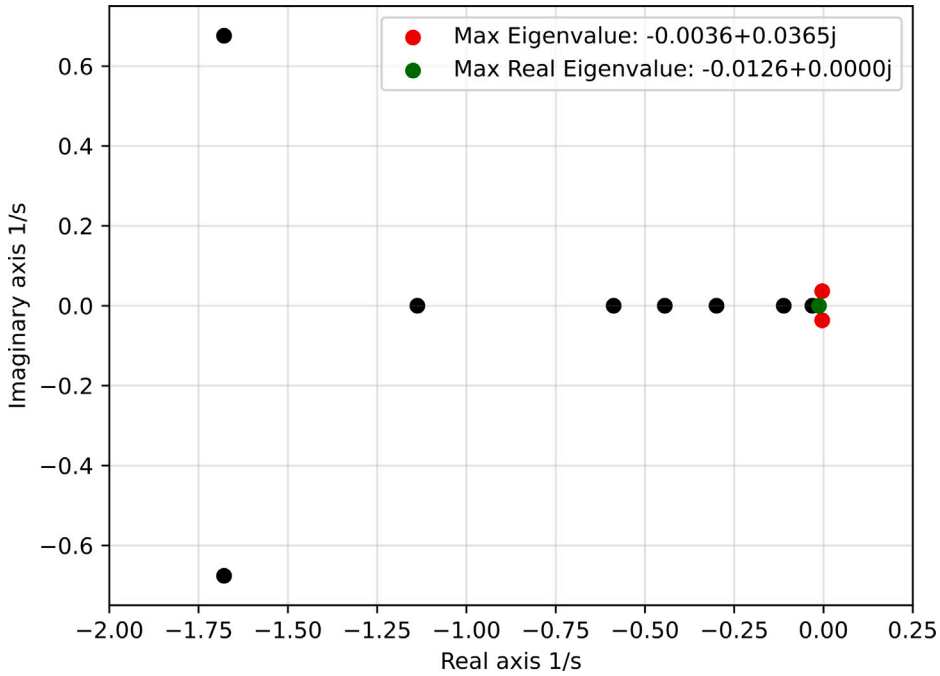

Fig. 5. Eigenvalues of the SCWR dynamic matrix **A**: all eigenvalues have negative real part, and the system presents two pairs of complex conjugate eigenvalues, indicating oscillating behaviour following a perturbation. The eigenvalues with the smallest real part are highlighted in red.

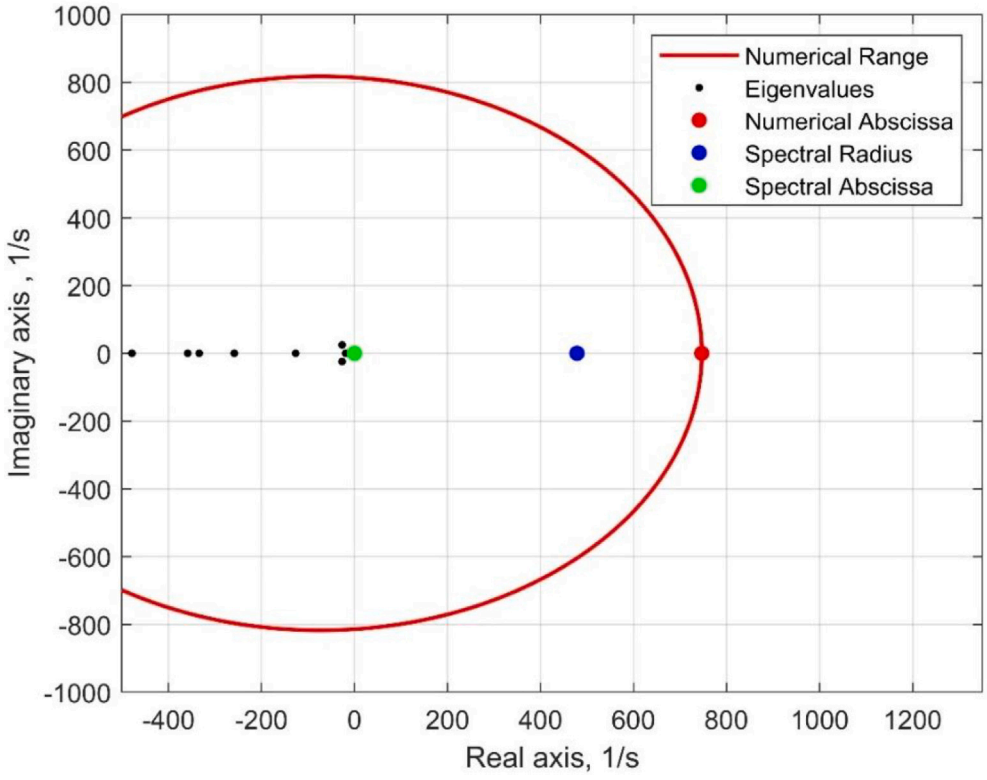

Fig. 6. Numerical range (red line), eigenvalue with modulus equal to the spectral radius (blue dot), spectral abscissa (green dot), numerical abscissa (red dot). The numerical range crosses into the right complex half-plane, indicating the possibility of transient growth according to the perturbation magnitude.

Fig. 6 shows the numerical range of **A**. As it crosses into the right half-plane, a transient growth of the perturbation following even small deviations from the steady state is possible. Other quantities reported on the plot are the spectral radius, which is defined as the absolute value of the eigenvalue with largest modulus (equal to 478.35); the spectral abscissa, which is defined as the real part of the rightmost eigenvalue (equal to ω_1); and the numerical abscissa, which is the largest protrusion of the numerical range into the right half-plane (equal to 746.68). Another important quantity to predict the possibility of transient growth is the departure from normality of the dynamic matrix **A**, defined as the Frobenius norm of $\boldsymbol{S} - l_i$, where $\boldsymbol{S}$ is the Schur factor of **A** and l_i is the diagonal of $\boldsymbol{S}$: the higher this number is, the farthest from orthogonality is the dynamic matrix. For the SCWR model, this value is equal to 1688.94, meaning that the matrix **A** is

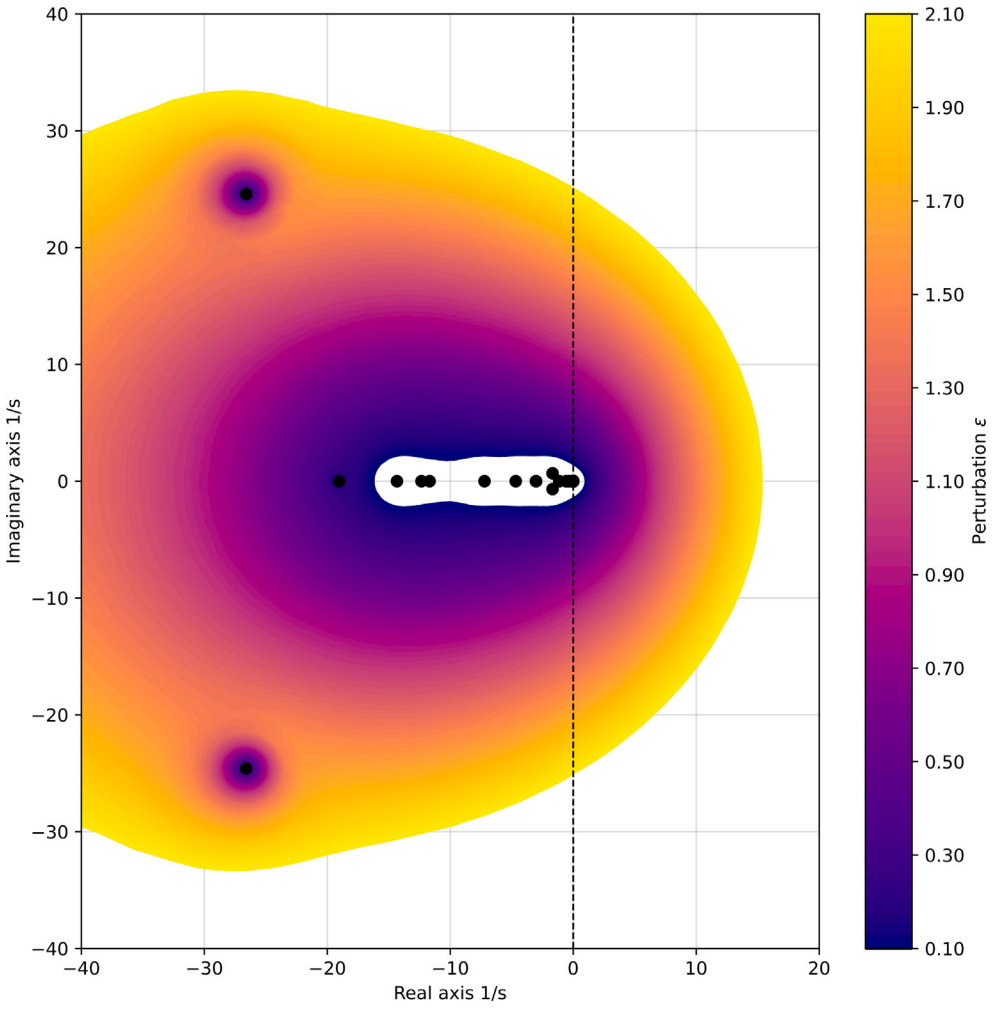

Fig. 7. Contour plots (pseudospectra) of the Euclidean norm for different values of the perturbation ε. The colour bar shows the norm of the perturbation on the logarithmic scale ($\log(\varepsilon)$), focusing on the largest magnitude eigenvalues (i.e., the ones whose variations impact the most the non-modal stability).

severely non-orthogonal and therefore that the temporal behaviour of $G(t)$ differs from that of $G(t)$, justifying the need for non-modal analysis.

Figs. 7 and 8 show the contour levels (i.e., the pseudospectra) for different values of the generic perturbation ε. Only the largest eigenvalues have been considered, as their variations impact non-modal stability the most. As shown in the figure, even perturbations of small magnitude (such as $\varepsilon = 0.0005$, corresponding to $\log(\varepsilon) = -3.3$) shifts the contour levels into the right half-plane, confirming the possibility of transient growth even for small perturbations of the dynamic matrix $\mathbf{A}$. However, large enough perturbations cause the pseudo-spectrum of 'safe' eigenvalues with strong negative real part to cross into the right half-plane, as seen for the eigenvalue $\omega = -20$ on the left-most plot.

Transient growth is now made clear by looking at Fig. 9, which displays the transient behaviour of the norm of matrix power $\|\mathbf{A}^k\|$ on a logarithmic scale on the left, and the largest energy increase $G(t)$ on a linear scale, on the right, for a perturbation $\log(\varepsilon) = -3$. For the matrix power $\mathbf{A}^k$, the least stable eigenvalue slightly underestimates the matrix power, especially at the beginning where initial growth is evident; as the spectral radius is greater than one, the matrix power does not converge.

For $G(t)$, seen in Fig. 10, a transient growth is observed. After the first peak at $t = 35$ s, the growth is repeated with decreasing magnitude and with constant period equal to roughly 86 s, until stability is reached after roughly $t = 1500$ s: this implies that following a generic perturbation from the steady state, the SCWR stabilises around the new equilibrium state after roughly 25 min. This type of growth is different from the one observed for the PWR model in Introini et al. (2020), in which a smooth decrease of $G(t)$ was observed. This could be related to the behaviour of thermo-dynamic properties around the critical point, which show rapid changes in the so-called pseudo-boiling region. Verification in this sense is currently foreseen. Regarding the value of 86 s, it is worth mentioning how this number is actually one order of magnitude larger compared to typical periods for DWO-like oscillations in supercritical systems (Upadhyay et al., 2018): given that, as seen later when decoupling the contributions of neutronics and thermal-hydraulics, the former is slower, it could be that the coupling has a slowing-down effect compare to pure DWO-like oscillations. Further slowing-down may be caused by thermal inertia due to energy storage in the steel rod. Given this result, more detailed studies will be performed in this sense.

Up to now, generic perturbations ε have been used; in the following, instead, the effect of a perturbation on specific parameters of the matrix $\mathbf{A}$ will be considered to gather more details regarding the nature of the observed transient growth. First, perturbed reactivity feedback coefficients are considered, and the behaviour of $\|\exp(\mathbf{A}t)\|$ following a 100% increase of the nominal values of α_f (−1.4 pcm/°C), α_c (1 pcm/(kg/m^3)) and α_w (7.5 pcm/(kg/m^3)), respectively is reported in Fig. 11. In all three cases, transient growth is observed, with different temporal behaviour. For a perturbation on α_f (red line), the maximum of the growth is higher, however the oscillations in the transient growth are much less pronounced compared to the other two cases, with lower frequency, and they exhaust after roughly 18 min. Conversely, the

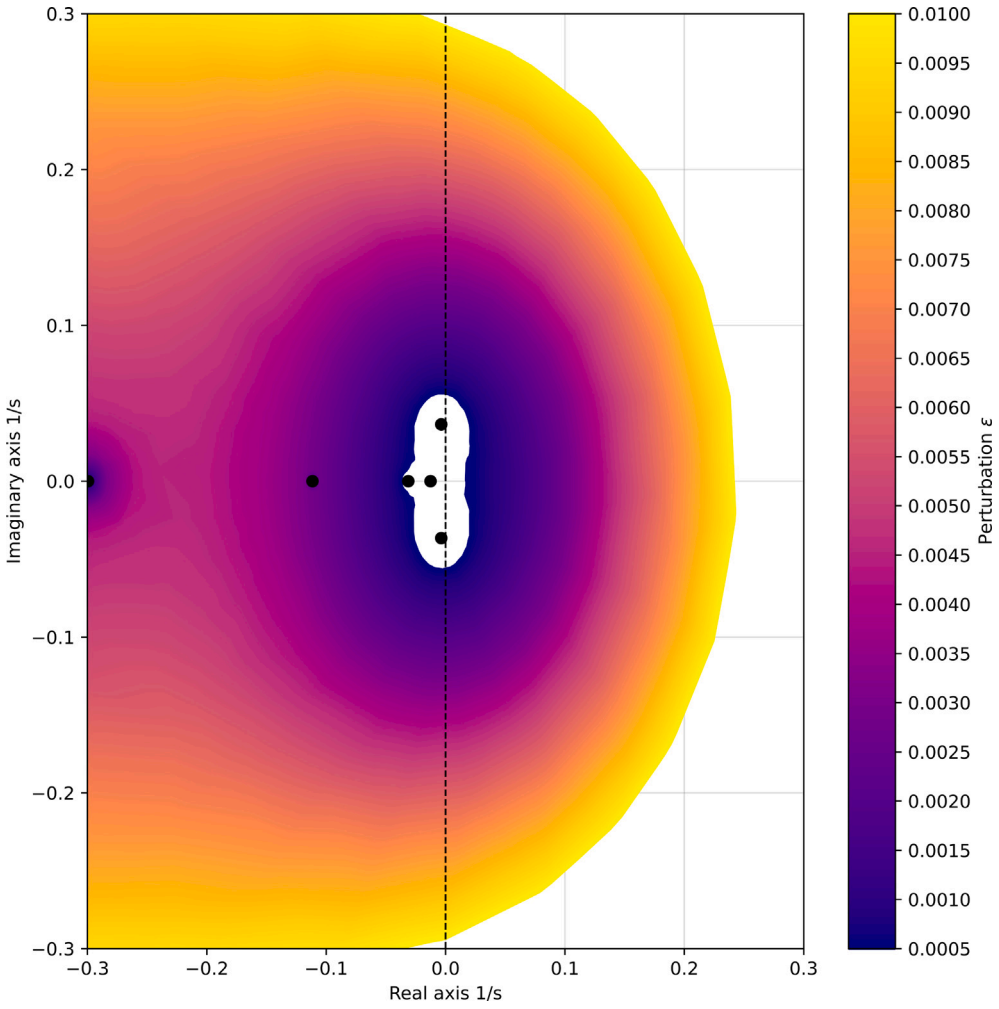

Fig. 8. Contour plots (pseudospectra) of the Euclidean norm for different values of the perturbation ε, focusing on small perturbations and their effect on the larger eigenvalues. The colour bar shows the norm of the perturbation on the logarithmic scale ($\log(\varepsilon)$), focusing on the largest magnitude eigenvalues (i.e., the ones whose variations impact the most the non-modal stability).

behaviour for variations in α_c (blue line) and α_w (green line) is quite different. Oscillations are much more pronounced, albeit with lower maximum peak, with higher frequency, and they exhaust much slower compared to those caused by a perturbation on α_c: oscillations in the energy of the perturbation persists even after 30 min, and asymptotic stability is reached much slower. This difference in behaviour seems to point that this oscillatory behaviour of the maximum perturbation energy is caused mainly by thermal-hydraulics.

To confirm this result, Fig. 12 considers the contributions of the two physics, neutronics and thermal-hydraulics, separately: namely, the problem is decoupled, resulting in two indirectly-coupled matrices $\mathbf{A}_N$ and $\mathbf{A}_{TH}$ for neutronics and thermal-hydraulics respectively, which are then perturbed separately, with feedback being provided by the unperturbed component. For both cases, oscillatory transient growth is observed: the neutronics component, however, exhausts much earlier compared to the thermal-hydraulic one, which instead mimics the behaviour of the coupled system, confirming that the oscillatory behaviour is caused by the thermal-hydraulics components.

5. Conclusions

In this work, non-modal stability analysis theory was applied to a mono-dimensional model of the Supercritical Water Reactor core, considering the short-term dynamic response of the system to a perturbation. The results show that even considering small disturbances of the free-dynamics matrix $\mathbf{A}$, a transient growth of the energy $G(t)$ is observed. This implies that the least stable eigenvalue ω_1 does not give meaningful information when describing the short-term dynamics. Indeed, the plot in time of the exponential matrix $\exp(\mathbf{A}t)$ shows multiple peaks with decreasing amplitude, with a period of $\sim$ 86 s, whereas the steady state is reached on a timescale of $\sim$ 1500 s. This periodicity of the transient growth could be related to DWO instabilities, indicating potential oscillations, following the perturbation, that then exhaust in roughly 25 min (by imposing a constant density the system becomes unstable).

In more details, the oscillatory behaviour seems to be imputable to thermal-hydraulic perturbations: indeed, by decoupling the two physics, neutronics perturbations present a much smoother decay to asymptotic stability, with less and smaller oscillations compared to thermal-hydraulics perturbations. Additionally, by looking at the effect of perturbation to the coupling coefficients (therefore, the response of the system to variations in the fuel temperature and water density), the oscillatory behaviour is much more pronounced for the feedback coefficients of the coolant and the water rod, with higher-frequency oscillations and a much slower decay to asymptotic stability. As a results, it is safe to assume that thermal-hydraulic instabilities are responsible for transient growth of the perturbation.

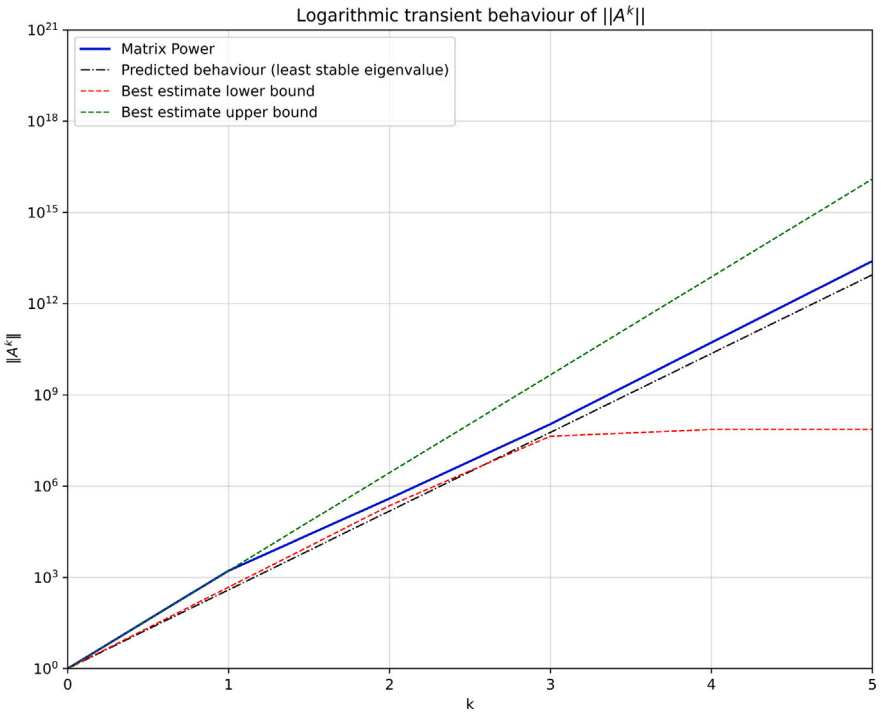

Fig. 9. Logarithmic transient growth of the matrix power $\|\mathbf{A}^k\|$ compared to the one predicted by the least stable eigenvalue, the best estimate upper and lower bounds.

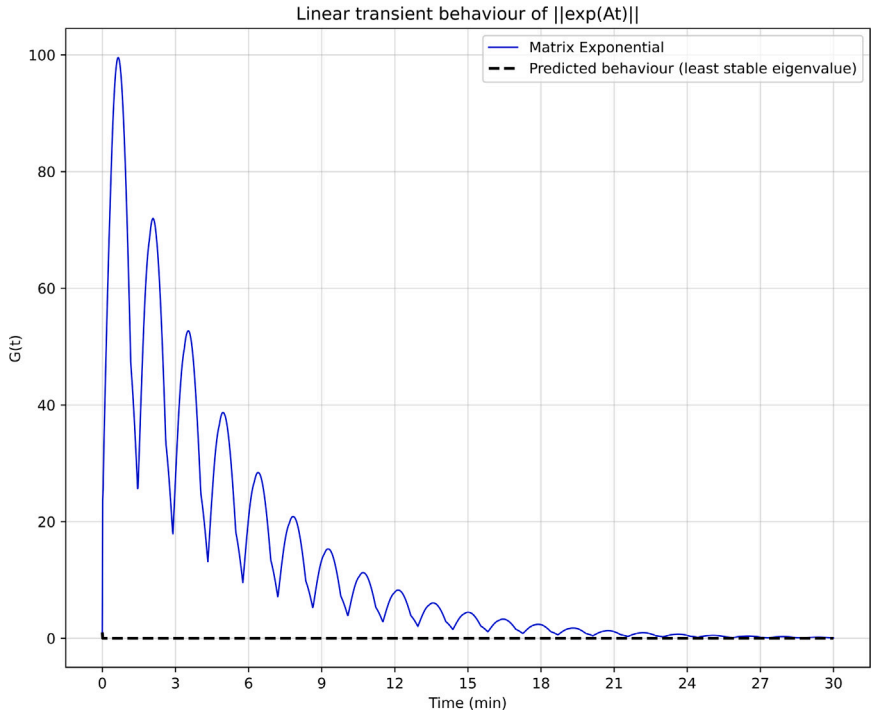

Fig. 10. (Linear transient growth of the perturbation energy $\|\exp(\mathbf{A}t)\|$ with respect to time, compared to the polynomial fit and the behaviour predicted by the least stable eigenvalue.

From an engineering perspective, identifying the possible occurrence of such a response to a perturbation is of paramount importance: whereas, by its nature, the transient growth occurs in a very small time frame, immediately after the disturbance, if repeated in time this kind of behaviour might affect the wear-and-tear of the components. When setting operative margins, it is recommended not only to ensure long-term stability, but also to minimise, as much as possible, the occurrence of transient growth phenomena. Indeed, this kind of stability analysis approach can be used to perform sensitivity analysis on the system parameters, to identify which parameter perturbation causes the largest

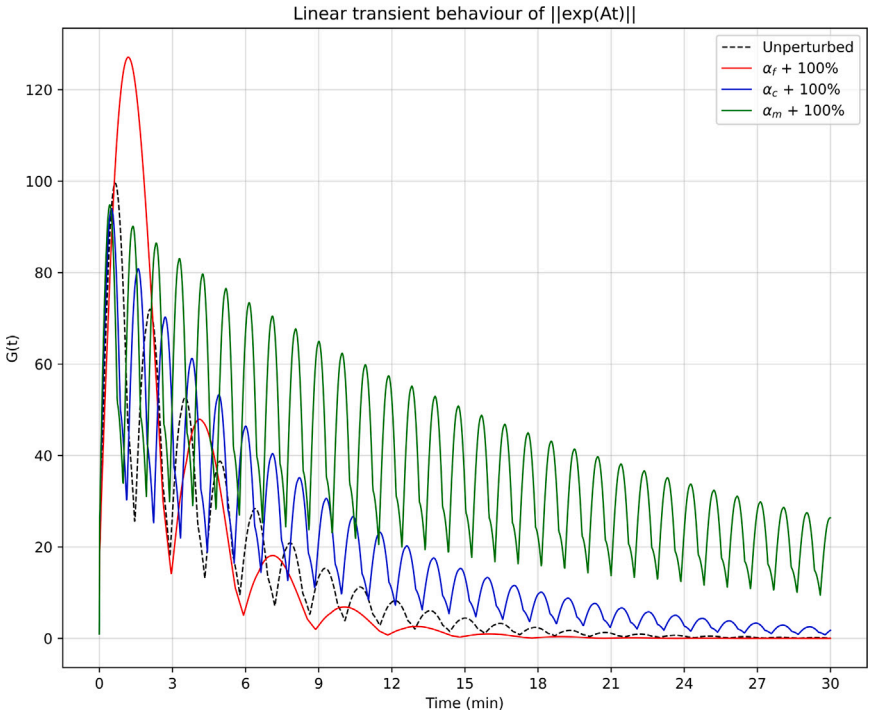

Fig. 11. Linear transient growth of the perturbation energy with respect to time, for perturbations in α_f (red line), α_c (blue line) and α_w (green line): oscillations are much more pronounced for the latter two, indicating that they might be mainly caused by the thermal-hydraulic component.

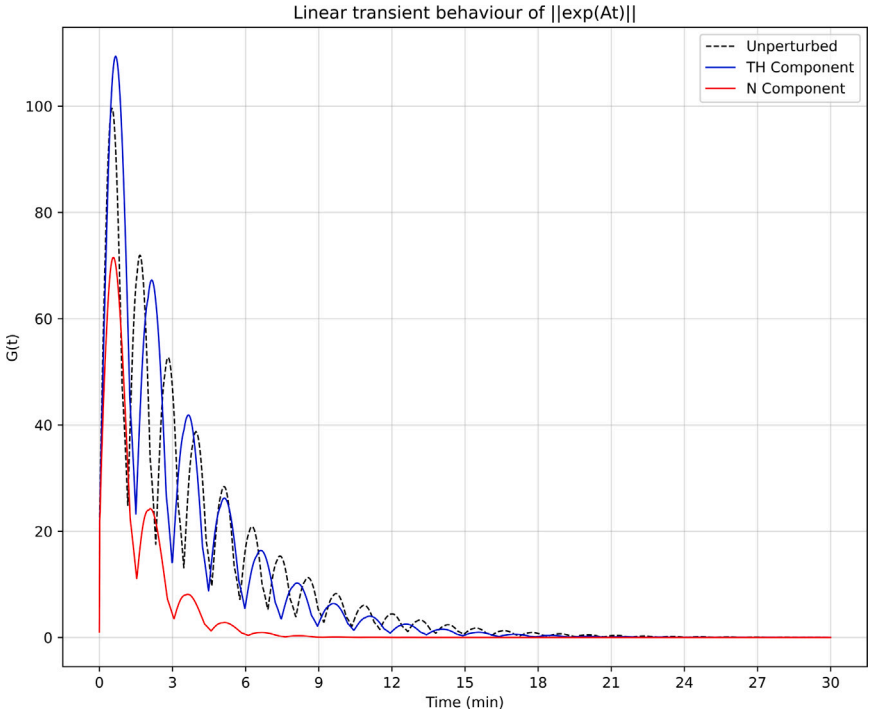

Fig. 12. Linear transient growth of the perturbation energy with respect to time, for perturbations in the neutronics component $\mathbf{A}_N$ (red line) and in the thermal-hydraulic component $\mathbf{A}_{TH}$ (blue line) only: the oscillatory behaviour is much more pronounced for the latter, indicating that it is caused mainly by the thermal-hydraulic component and hence it is related to thermal-hydraulic instabilities.

energy growth, as well as to consider the influence of noisy and perturbed external inputs on the dynamic response of the system. Future works will delve into more details, further improving the model (for example adding the effective hydraulic resistance of the channel).

Nomenclature

Acronyms

BWR	Boiling Water Reactor
DNB	Departure of Nucleate Boiling
DWO	Density Wave Oscillations
LWR	Light Water Reactor
SCWR	Super-critical Water Reactor
SVD	Singular Value Decomposition

Latin Symbols

$\mathbf{A}$	System (free-dynamics) matrix
A	Cross-sectional area (m^2)
$\mathbf{B}$	Input matrix
$\mathbf{C}$	Output matrix
c	Specific heat (J/kgK)
$\mathbf{D}$	Feedforward matrix
d_h	Hydraulic diameter (m)
dz	Node height (cm)
$\mathbf{E}$	Perturbation matrix
f	Friction factor
$G(t)$	Maximum amplification of perturbation energy
H	Core total height (m)
h	Convective heat transfer coefficient (W/m^2K)
$\mathbf{I}$	Identity matrix
κ	Thermal conductivity
L	Heated length (m)
l_i	Diagonal of S
m_f	Mass (kg)
$\dot{m}$	Mass flow rate (kg/s)
Nu_b	Bulk Nusselt number
p	Pressure (Pa)
$\bar{Pr}_b$	Cross-average bulk Prandtl number
$\dot{Q}$	Power produced (W)
q	Neutron external source
R_{pin}	Fuel pin outer radius (m)
Re_b	Bulk Reynolds number
$\boldsymbol{S}$	Schur factor of $\mathbf{A}$
S	External surface
T	Temperature (K)
V	Volume (m^3)
v	Water velocity (m/s)
$\mathbf{W}$	Eigenvector matrix
$x(t)$	Time-dependent system state
$y(t)$	Time-dependent system output
y_0	Output initial condition

Greek Symbols

α	Feedback coefficient
β	Delayed neutron fraction (pcm)
ΔP_p	Pressure drop between (Pa)
δ	Density (kg/m^3)
ϵ	Perturbation magnitude
η	Normalised precursor density
$\boldsymbol{\Lambda}$	Eigenvalue matrix
Λ	Mean neutron generation time (s)
$\Lambda_\epsilon(\mathbf{A})$	ϵ-pseudospectrum of $\mathbf{A}$
λ	Precursor decay constant
ρ	Reactivity (pcm)
ψ	Normalised power density
ω_1	Real part of the least stable eigenvalue of $\mathbf{A}$

Subscripts and Superscripts

b	Liquid bulk
c	Coolant channel
f	Fuel
i	Node index
k	Precursor group index
LP	Lower plenum
s	Water rod steel surface
w	Water rod channel
0	Nominal values

CRediT authorship contribution statement

Carolina Introini: Writing – original draft, Visualization, Software, Methodology, Investigation, Formal analysis. **Antonio Cammi:** Writing – review & editing, Validation, Supervision, Conceptualization. **Eric Cervi:** Writing – review & editing, Software. **Laura Savoldi:** Writing – review & editing.

Declaration of competing interest

The authors declare that they have no known competing financial interests or personal relationships that could have appeared to influence the work reported in this paper.

Appendix. SCWR model equations

A.1. Non-linear model equations

The model equations are taken from Cervi and Cammi (2018), and hereby reported for completeness, starting from the time-dependent energy balances of the core.

- **Fuel energy balance**:

$$m_{f,i}c_f\frac{dT_{f,i}}{dt} = \dot{Q}_i - h_{f,i}S_{f,i}(T_{fo,i} - T_{c,i}), \tag{A.1}$$

with $m_{f,i}$ as the total mass of the fuel in node i, c_f the fuel specific heat, $h_{f,i}$ the convective heat transfer coefficient between fuel and coolant, $S_{f,i}$ the external surface of the node i fuel-side and $\dot{Q}_i$ is the power produced by the fraction of fuel contained in node i. Regarding the fuel temperature, assuming a uniformly distributed radial power source in the fuel pins (see Eq. (A.17)) and neglecting the thermal resistance of the gap and the cladding, the following relation holds:

$$T_{f,inner} = T_{f,o} + \frac{1.4\cdot\dot{Q}_i}{8\kappa_f V_{f,i}} r\cdot\cos\frac{\pi(i\cdot dz - H/2)}{H}R_{pin}^2, \tag{A.2}$$

with κ_f as the fuel thermal conductivity, $V_{f,i}$ as the volume of fuel contained in node i and R_{pin} as the fuel pin outer radius.

- **Coolant energy balance**

$$\frac{d(\delta_{c,i}c_cT_{c,i})}{dt} = \frac{h_{f,i}S_{f,i}(T_{fo,i} - T_{c,i}) - h_{c,i}S_{c,i}(T_{c,i} - T_{s,i})}{A_c dz} - \frac{\delta_{c,out,i}v_{c,out,i}c_{c,out}T_{c,out,i} + \delta_{c,in,i}v_{c,in,i}c_{c,in}T_{c,in,i}}{dz}, \tag{A.3}$$

with $\delta_{c,i}$ as the coolant density, c_c as the coolant specific heat, $h_{c,i}$ as the convective heat transfer coefficient between the coolant and the water rod steel surface, $S_{c,i}$ as the external water rod surface, $v_{c,i}$ the coolant velocity, A_c being the coolant channel cross sectional area and dz being the node height.

- **Water rod surface energy balance**

$$m_{s,i}c_s\frac{dT_{s,i}}{dt} = h_{c,i}S_{c,i}(T_{c,i}-T_{s,i}) - h_{w,i}S_{w,i}(T_{s,i}-T_{w,i}), \tag{A.4}$$

with $m_{s,i}$ the mass of the steel surface in node i, c_s the steel specific heat, $h_{w,i}$ the convective heat transfer coefficient between the water rod steel surface and the water rod, $S_{w,i}$ the inner water rod surface.

- **Water rod energy balance**

$$\frac{d(\delta_{w,i}c_wT_{w,i})}{dt} = \frac{h_{w,i}S_{w,i}(T_{s,i}-T_{w,i})}{A_w dz} - \frac{\delta_{w,out,i}v_{w,out,i}c_{w,out}T_{w,out,i} + \delta_{w,in,i}v_{w,in,i}c_{w,in}T_{w,in,i}}{dz}, \tag{A.5}$$

with $\delta_{w,i}$ the water rod density, c_w the water rod specific heat, A_w the water rod cross sectional area and $v_{w,i}$ the water rod velocity.

Continuity dynamics for the coolant and the water rod are expressed as:

- **Coolant continuity**:

$$\frac{d\delta_{c,i}}{dt} = \frac{\delta_{c,in,i}v_{c,in,i} - \delta_{c,out,i}v_{c,out,i}}{dz} \tag{A.6}$$

- **Water rod continuity**:

$$\frac{d\delta_{w,i}}{dt} = \frac{\delta_{w,in,i}v_{w,in,i} - \delta_{w,out,i}v_{w,out,i}}{dz} \tag{A.7}$$

In the lower plenum, the water rods and the downcomer flows mix in this region, and the resulting flow turns upward into the coolant channels. Under the instantaneous mixing approximation, neglecting the time delay of the mixing, and considering the downcomer mass flow rate $\dot{m}_d$, specific enthalpy h_d and volume V_{LP}:

- **Lower plenum mass balance**:

$$V_{LP}\frac{d\delta_{c,in,M}}{dt} = \delta_{w,out,M}A_wv_{w,out,M} - \delta_{c,in,M}A_cv_{c,in,M} - \dot{m}_D \tag{A.8}$$

- **Lower plenum energy balance**:

$$V_{LP}\frac{d\delta_{c,in,M}c_cT_{c,in,M}}{dt} = \delta_{w,out,M}A_wv_{w,out,M}c_wT_{w,out,M} - \delta_{c,in,M}A_cv_{c,in,M}c_cT_{c,in,M} - \dot{m}_Dh_d \tag{A.9}$$

The momentum balance of the coolant and water rods allows to complete the description of the open-loop channel dynamics:

- **Coolant channel momentum balance**:

$$\frac{dm_{c,i}v_{c,i}}{dt} = A_c(\delta_{c,in,i}v_{c,in,i}^2 - \delta_{c,out,i}v_{c,out,i}^2 + p_{c,in,i} - p_{c,out,i} - p_{c,i}g\Delta z - \delta_{c,i}v_{c,i}^2\frac{dz}{2d_{h,c}}f_{c,i} + \Delta P_i), \tag{A.10}$$

with p_c as the coolant pressure, g as the gravity acceleration, $d_{h,c}$ as the hydraulic diameter of the coolant channel, f_c as the overall friction factor for the coolant.

- **Water rod channel momentum balance**:

$$\frac{dm_{w,i}v_{w,i}}{dt} = A_w(\delta_{w,in,i}v_{w,in,i}^2 - \delta_{w,out,i}v_{w,out,i}^2 + p_{w,in,i} - p_{w,out,i} - p_{w,i}g\Delta z - \delta_{w,i}v_{w,i}^2\frac{dz}{2D_{h,w}}f_{w,i} + \Delta P_i), \tag{A.11}$$

with p_w as the water rod pressure, $d_{h,w}$ as the hydraulic diameter of the water rod channel, f_w as the overall friction factor for the water rod.

From these two equations, the expression for the pressure drops over a node can be obtained, and a constant pressure drop boundary condition ΔP_p is assumed between the feedwater pump and the turbine control valve for the out-core dynamics, including the pump gain and the exit valve pressure drop.

Regarding the convective heat transfer between the wall and the supercritical flow, several correlations were compared against reference data from Zhao (2005) in Cervi (2016): from their analysis, the Mokry correlation (Pioro and Mokry, 2011) was selected for the present model:

$$Nu_b = 0.0061\cdot Re_b^{0.904}\bar{Pr}_b^{.684}\left(\frac{\rho_s}{\rho_b}\right)^{0.564} \tag{A.12}$$

where the Reynolds number is calculated at the bulk-fluid temperature, based on the equivalent diameter, whereas the Prandtl number is computed as a cross-section average, accounting for the variations of the thermo-physical properties within the cross section of the channel (an iterative procedure must be used, given the dependency on the wall and bulk temperatures):

$$\bar{Pr} = \frac{\mu\bar{c_p}}{\kappa} = \frac{\mu}{\kappa}\frac{h_s-h_b}{T_s-T_b} \tag{A.13}$$

For neutronics, the normalised point kinetics equations are used:

$$\frac{d\psi}{dt} = \frac{\rho-\beta}{\Lambda}\psi + \sum_{i=6}^{6}\lambda_k\eta_k + q \tag{A.14}$$

$$\frac{d\eta_k}{dt} = \frac{\beta_k}{\Lambda}\psi - \lambda_k\eta_k \tag{A.15}$$

$$\rho = \rho_{ext} + \alpha_f(T_f - T_f^0) + \alpha_c(\delta_c - \delta_c^0) + \alpha_w(\delta_w - \delta_w^0), \tag{A.16}$$

where ψ is the normalised power density, ρ is the system reactivity, β is the delayed neutron fraction, Λ is the mean neutron generation time, q is an external source, η_k is the normalised precursor density for group k, λ_k is the decay constants for precursors of group k, ρ_{ext} is the external reactivity inserted by the operator, α indicates the feedback coefficient for fuel temperature, coolant and water rod density, T_f, T_c and T_w are power-averaged quantities. Since no information on the shape of the neutron flux and of the volumetric power is available, an axial cosine profile is adopted:

$$\dot{Q}_i = \frac{\dot{Q}}{L}dz\cdot r\cdot 1.4\cdot\cos\frac{\pi(i\cdot dz - H/2)}{H}, \tag{A.17}$$

where $\dot{Q}$ is the total power, L is the heated length, Δz is the node height and H is the core total height. This relation holds for nodes $i > 30$ and $i < 457$, corresponding to the active length of the fuel (for which the factor r is set equal to 1); for nodes outside this range, corresponding to the plenum regions, $r = 0$.

A.2. Core pressure drop

The pressure drop over a node of the coolant channel and of the water rod can be obtained with the following relation:

$$\Delta P_i = \delta_{in,i}v_{in,i}^2 - \delta_{out,i}v_{out,i}^2 \pm \delta_i g dz - \frac{dz}{2D_h}\delta_i v_i^2 f_{dw,i}, \tag{A.18}$$

where the sign of the gravity term depends on the direction of the flow (positive for the water rod, negative for the coolant); D_h is the hydraulic diameter (0.0034 m for the coolant, 0.0328 m for the water rod). The frictional resistance coefficient is computed as (Kirillov et al., 1990):

$$f = (1.82\log Re_b - 1.64)^{-2}\left(\frac{\rho_s}{\rho_b}\right)^{0.4} \tag{A.19}$$

For the first node of the upward channel, the concentrated pressure drop due to the inlet orifice must also be included:

$$\Delta P_o = -\frac{1}{2}K_{in}\rho_{c,in,1}v_{c,in,1}^2 \tag{A.20}$$

From the literature, the inlet orifice coefficient is equal to 115 (Zhao, 2005). Overall, the total pressure drop is equal to 0.141 MPa, in good agreement with the target value of 0.15 MPa (Buongiorno and MacDonald, 2003). The total core pressure drop acts

A.3. Model linearisation

The resulting system of equations is then linearised by expressing all variables in terms of their variations with respect to a stationary point, substituting them into the non-linear equations and neglecting the superior order infinitesimals. In state-space representation, the resulting linear system can be written as:

$$\dot{\mathbf{x}} = \mathbf{A}\mathbf{x} + \mathbf{B}\mathbf{u} \tag{A.21}$$

$$\mathbf{y} = \mathbf{C}\mathbf{x} + \mathbf{D}\mathbf{u} \tag{A.22}$$

where **A** is the dynamic matrix which describes the (free) dynamic evolution of the system, **B** is the input matrix, containing the relationship between state variables and input quantities, **C** is the output matrix, containing the relationship between state variables and output quantities (for example, the algebraic relation between average and outlet temperature) and **D** is the feedforward matrix, containing the relationship between output and input quantities. The unknown state variable vector **x** (quantities described by differential equations), output vector **y** (quantities described by algebraic relations, if the state variable coincides with the output variable then the corresponding coefficient in matrix **C** is one) and input vector **u** of the resulting system are the following:

$$\begin{aligned}
&\mathbf{x} = [\psi, \eta_k, T_f, T_c, T_s, T_w, \delta_c, \delta_w, v_c, v_w, \delta_{c,in,M}, T_{c,in,M}]; \\
&\mathbf{y} = [\psi, \eta_k, T_{fo}, T_{c,out}, T_{c,in}, T_{w,out}, T_{w,in}, v_{c,out}, v_{c,in}, v_{w,out}, w_{w,in}]; \\
&\mathbf{u} = [\rho_{ext}, T_{w,in}, \dot{m}_d h_d, \Delta P_p],
\end{aligned} \tag{A.23}$$

with:

- $T_f = 1/2 \cdot (T_{f,inner} + T_{f,o})$ as the fuel temperature (see Eq. (A.2));
- $T_c = 1/2 \cdot (T_{c,in} + T_{c,out})$ as the coolant channel temperature;
- T_s as the water rod steel surface temperature;
- $T_w = 1/2 \cdot (T_{w,in} + T_{w,out})$ as the water rod channel temperature;
- $v_c = 1/2 \cdot (v_{c,in} + v_{c,out})$ as the coolant channel velocity;
- $v_w = 1/2 \cdot (v_{w,in} + v_{w,out})$ as the water rod channel velocity;
- ρ_{ext} as the external reactivity inserted by movement of the control rods;
- $T_{w,in} = 280$ °C, as the water rod inlet temperature, which represents the out-of-core energy dynamics, not included in the present model;
- $\dot{m}_d h_d$ as the downcomer conditions;
- ΔP_p as the pressure drop condition between the feedwater pump and the turbine control valve

The complete linear equations describing the model, along with additional details on their derivation, can be found in Cervi (2016); here, a summary is provided. To linearise the nonlinear system of ODE, all the state and output variables in the (differential) Eq. (A.1) to (A.14) are expressed in terms of their variations with respect to the stationary point. Therefore, considering a generic variable q, except for density:

$$q_i(t) = q_i^0 + \partial q_i(t). \tag{A.24}$$

The variations of the density are expressed in terms of temperature changes:

$$\partial\delta_i = \xi_i^0 \partial T_i, \tag{A.25}$$

where ξ_i^0 is the derivative of the density with respect to the corresponding temperature, evaluated at stationary state (Yang, 2005)- All the mean representative thermo-physical properties have been calculated as average of the values obtained from the stationary analysis. Substituting the linearised variables in the thermal-hydraulics equations, neglecting the superior-order infinitesimal and Laplace-transforming, the following linear equations can be found:

- **Fuel energy balance**:

$$s \cdot m_{f,i} c_f \delta\widetilde{T}_{f,i} = \delta\widetilde{\psi} F_i \cdot \dot{Q}_o - h_{f,i} S_{f,i} (\delta\widetilde{T}_{fo,i} - \delta\widetilde{T}_{ci}) \tag{A.26}$$

- **Coolant energy balance**:

$$s(\delta_{c,i}^o c_{c,i}^o + h_{c,i}^o \xi_{c,i}^o)\partial\widetilde{T}_{c,i} = \frac{h_{f,i} S_{f,i}}{A_c dz}(\partial\widetilde{T}_{fo,i} - \partial\widetilde{T}_{c,i}) - \frac{h_{c,i} S_{c,i}}{A_c dz}(\partial\widetilde{T}_{c,i} - \delta T_{s,i}) \tag{A.27}$$

$$\begin{aligned}
&+ \left(\frac{v_{c,in,i}^o h_{c,in,i}^o \xi_{c,in,i}^o}{dz} + \frac{\rho_{c,in,i}^o v_{c,in,i}^o c_{c,in,i}^o}{dz}\right)\partial\widetilde{T}_{c,in,i} \\
&+ \frac{\rho_{c,in,i}^o h_{c,in,i}^o}{dz}(2\partial\widetilde{v}_{c,i} - \partial\widetilde{v}_{c,in,i+1}) - \frac{\rho_{c,out,i}^o h_{c,out,i}^o}{dz}\partial v_{c,in,i+1} \\
&- \left(\frac{v_{c,out,i}^o h_{c,out,i}^o \xi_{c,out,i}^o}{dz} - \frac{\rho_{c,out,i}^o v_{c,out,i}^o c_{c,out,i}^o}{dz}\right)(2\partial\widetilde{T}_{c,i} - \partial\widetilde{T}_{c,in,i})
\end{aligned}$$

- **Water rod surface energy balance**:

$$s \cdot m_{s,i} c_s \partial\widetilde{T}_{s,i} = h_{c,i} S_{c,i}(\partial\widetilde{T}_{c,i} - \partial\widetilde{T}_{s,i}) - h_{w,i} S_{w,i}(\partial\widetilde{T}_{s,i} - \partial\widetilde{T}_{w,i}) \tag{A.28}$$

- **Water rod energy balance**:

$$\begin{aligned}
&s(\rho_{w,i}^o c_{w,i}^o + h_{w,i}^o \xi_{w,i}^o)\partial\widetilde{T}_{w,i} = \frac{h_{w,i} S_{w,i}}{A_w dz}(\partial\widetilde{T}_{s,i} - \partial\widetilde{T}_{w,i}) \\
&+ \left(\frac{v_{w,in,i}^o h_{w,in,i}^o \xi_{w,in,i}^o}{dz} + \frac{\rho_{w,in,i}^o v_{w,in,i}^o c_{w,in,i}^o}{dz}\right)\partial\widetilde{T}_{w,in,i} \\
&+ \frac{\rho_{w,in,i}^o h_{w,in,i}^o}{dz}(2\partial\widetilde{v}_{w,i} - \partial\widetilde{v}_{w,in,i+1}) - \frac{\rho_{w,out,i}^o h_{c,out,i}^o}{dz}\partial\widetilde{v}_{w,in,i+1} \\
&- \left(\frac{v_{w,out,i}^o h_{w,out,i}^o \xi_{w,out,i}^o}{dz} - \frac{\rho_{w.out,i}^o v_{w,out,i}^o c_{w,out,i}^o}{dz}\right)(2\partial\widetilde{T}_{w,i} - \partial\widetilde{T}_{w,in,i})
\end{aligned} \tag{A.29}$$

- **Coolant continuity**:

$$\begin{aligned}
&s \cdot \xi_{c,i}^o \partial\widetilde{T}_{c,i} = \frac{v_{c,in,i}^o \xi_{c,in,i}^o}{dz}\partial\widetilde{T}_{c,in,i} + \frac{\rho_{c,in,i}^o}{dz}(2\partial\widetilde{v}_{c,i} - \partial\widetilde{v}_{c,in,i+1}) \\
&- \frac{v_{c,out,i}^o \xi_{c,out,i}^o}{dz}(2\partial\widetilde{T}_{c,i} - \partial\widetilde{T}_{c,in,i}) - \frac{\rho_{c,out,i}^o}{dz}\partial\widetilde{v}_{c,in,i+1}
\end{aligned} \tag{A.30}$$

- **Water rod continuity**:

$$\begin{aligned}
&s \cdot \xi_{w,i}^o \partial\widetilde{T}_{w,i} = \frac{v_{w.in,i}^o \xi_{w,in,i}^o}{dz}\partial\widetilde{T}_{w,in,i} + \frac{\rho_{w,in,i}^o}{dz}(2\partial\widetilde{v}_{w,i} - \partial\widetilde{v}_{w,in,i+1}) \\
&- \frac{v_{w,out,i}^o \xi_{w,out,i}^o}{dz}(2\partial\widetilde{T}_{w,i} - \partial\widetilde{T}_{w,in,i}) - \frac{\rho_{w,out,i}^o}{dz}\partial\widetilde{v}_{w,in,i+1}
\end{aligned} \tag{A.31}$$

- **Lower plenum mass balance**:

$$\begin{aligned}
&s \cdot \xi_{c,in,M}^o V_{LP} \partial\widetilde{T}_{c,in,M} = \rho_{w,out,M}^o A_w (2\partial\widetilde{v}_{w,M} - \partial\widetilde{v}_{w,in,M}) \\
&+ A_w v_{w,out,M}^o \xi_{w,out,M}^o (2\partial\widetilde{T}_{w,M} - \partial\widetilde{T}_{w,in,M}) - \rho_{c,in,M}^o A_c \partial\widetilde{v}_{c,in,M} \\
&- A_c v_{c,in,M}^o \xi_{c,in,M}^o \partial\widetilde{T}_{c,in,M}
\end{aligned} \tag{A.32}$$

- **Lower plenum energy balance**:

$$\begin{aligned}
&s \cdot V_{LP} h_{c,in,M}^o \xi_{c,in,M}^o \partial\widetilde{T}_{c,in,M} + s\rho_{c,in,M}^o V_{LP} c_{c,in,M}^o \partial T_{c,in,M} = \\
&= \rho_{w,out,M}^o A_w h_{w,out,M}^o (2\partial\widetilde{v}_{w,M} - \partial v_{w,in,M}) \\
&+ A_w v_{w,out,M}^o h_{w,out,M}^o \xi_{w,out,M}^o (2\partial\widetilde{T}_{w,M} - \partial\widetilde{T}_{w,in,M}) \\
&+ \rho_{w,out,M}^o A_w v_{w,out,M}^o c_{w,out,M}^o (2\partial\widetilde{T}_{w,M} - \partial\widetilde{T}_{w,in,M}) \\
&- -\rho_{c,in,M}^o A_c h_{c,in,M}^0 \partial\widetilde{v}_{c,in,M} - A_c v_{c,in,M}^o h_{c,in,3}^o \xi_{c,in,3}^o \partial\widetilde{T}_{c,in,M} \\
&- \rho_{c,in,M}^o A_c v_{c,in,M}^o c_{c,in,M}^o \partial\widetilde{T}_{c,in,M}
\end{aligned} \tag{A.33}$$

In these equations, s is the Laplace transform independent variable and the superscript $\sim$ denotes the transformed dependent variable. Additionally, by expressing the linearised density as a function of the linearised temperature, the number of independent state variable (and therefore of independent equations) can be reduced.

The same linearisation procedure can be applied the point kinetics equations, resulting in the following linear equations:

$$s\partial\widetilde{\psi} = -\frac{\beta}{\Lambda}\partial\widetilde{\psi} + \sum_{i=1}^{6}\frac{\beta_i}{\Lambda}\partial\widetilde{\eta}_i + \frac{1}{\Lambda}\partial\widetilde{\rho}$$
$$s\partial\widetilde{\eta}_i = \lambda_i\partial\widetilde{\psi} - \lambda_i\partial\widetilde{\eta}_i \tag{A.34}$$

Data availability

Data will be made available on request.

References

Ambrosini, W., Sharabi, M., 2008. Dimensionless parameters in stability analysis of heated channels with fluids at supercritical pressures. Nucl. Eng. Des. 238, 1917–1929.

Buongiorno, J., MacDonald, P., 2003. Supercritical Water Reactor (SCWR) Progress Report for the FY-03 Generation-IV R&D Activities for the Development of the SCWR in the U.S.. Tech. Rep., Massachusetts Institute of Technology.

Cai, J., Ishiwatari, Y., Ikejiri, S., Oka, Y., 2009. Thermal and stability considerations for a supercritical water-cooled fast reactor with downward-flow channels during power-raising phase of plant startup. Nucl. Eng. Des. 239, 665–679.

Cervi, E., 2016. Stability Analysis of Density Wave Oscillations with Application to Boiling and Super-critical Water Nuclear Reactors (Master's thesis). Politecnico di Milano.

Cervi, E., Cammi, A., 2018. Stability analysis of the supercritical water reactor by means of the root locus criterion. Nucl. Eng. Des. 338, 137–157.

Dutta, G., Doshi, J., 2009. Nonlinear analysis of nuclear coupled density wave instability in time domain for a boiling water reactor core undergoing core-wide and regional modes of oscillations. Prog. Nucl. Energy 51, 769–787.

Gen-IV International Forum, 2023. GIF Annual Report 2023. Tech. Rep., Gen-IV International Forum.

Introini, C., Cammi, A., Giacobbo, F., 2020. Stability analysis of a zero-dimensional model of PWR core using non-modal stability theory. Ann. Nucl. Energy 146, 107624.

Kirillov, P.L., Yurev, Y.S., Bobkov, V.P., 1990. Handbook on the Thermohydraulic Calculations (Nuclear Reactors, Heat Exchangers, Steam Generators). Energoatomizdat, Moscow.

Lo Verso, M., Introini, C., Barucca, L., Caramello, M., Di Prinzio, M., Giacobbo, F., Savoldi, L., Cammi, A., 2024. Non-modal stability analysis of magneto-hydrodynamic flow in a single pipe. Fundam. Fo Plasma Phys.

March-Leuba, J., 1992. Density-wave Instabilities in Boiling Water Reactors. Tech. Rep., Oak Ridge National Laboratories.

Marquez, H.J., 2003. Nonlinear Control Systems: Analysis and Design. John Wiley & Sons.

Nise, N., 2010. Control System Engineering. John Wiley & Sons.

Ortega Gomez, T., 2009. Stability Analysis of the High-Performance Light Water Reactor (Ph.D. thesis). University of Karlsruhe.

Paul, S., 2019. On nuclear-coupled thermal-hydraulic instability analysis of Super-Critical-Light-Water-cooled-reactor (SCLWR). Prog. Nucl. Energy 117, 103051.

Pioro, I., Mokry, S., 2011. Heat Transfer - Theoretical Analysis, Experimental Investigations and Industrial Systems. InTech, InTech, 2011, Ch. Heat Transfer to Fluids at Supercritical Pressures.

Reddy, S.C., Schmidt, P., Henningson, D.S., 1993. Pseudospectra of the orr-sommerfield operator. J. Appl. Math. 53, 15–47.

Ruban, A., Gajjar, J., Walton, A., 2023. Hydrodynamic Stability Theory. In: Fluid Dynamics, Oxford Academy.

Schmidt, P., 2007. Nonmodal Stability Theory. Annu. Rev. Fluid Mech. 39, 129–162.

Schmidt, P., Henningson, D., 2001. Stability and Transition in Shear Flows. Springer-Verlag.

Schulenberg, T., Laurence, L., 2023. Chapter 8: SuperCritical Water-Cooled Reactors (SCWRs), second ed. In: Handbook of Generation IV Nuclear Reactors, Woodhead Publishing Series in Energy.

Singh, M., Saeed, M., Berrouk, A., 2022. Non linear stability analysis of supercritical water cooled reactor: Parallel channels configuration. Prog. Nucl. Energy 147, 104194.

Singh, M., Singh, S., Berrouk, A., 2021. On-linear analysis of the Density-Wave Oscillations and Ledinegg Instability in heated channel at supercritical condition. Prog. Nucl. Energy 133, 103639.

Su, Y., Feng, J., Zhao, H., Tian, W., Su, G., Qiu, S., 2013. Theoretical study on the flow instability of supercritical water in the parallel channels. Prog. Nucl. Energy 68, 169–176.

Trefethen, L., 1997. Pseudospectra of linear operators. SIAM Rev. 383–406.

Trefethen, L., Embree, M., 2005. Spectra and Pseudospectra: The Behaviour of Nonnormal Matrices and Operators. Princeton University Press.

Upadhyay, R., Kumar Rai, S., Dutta, G., 2018. Numerical analysis of density wave instability and heat transfer deterioration in a supercritical water reactor. J. Mech. Sci. Technol. 32, 1063–1070.

Yadigaroglu, G., 1970. An Experimental and Theoretical Study of Density-wave Oscillations in Two-phase Flow (Ph.D. thesis). Massachusetts Institute of Technology.

Yang, W.S., 2005. Initial Implementation of Multi-Channel Thermal-Hydraulics Capability in Frequency Domain SCWR Stability Analysis Code SCWRSA. Tech. Rep., Argonne National Laboratory.

Zhao, J., 2005. Stability Analysis of Supercritical Water-Cooled Reactors (Ph.D. thesis). Massachusetts Institute of Technology.